

Strain field of soft modes in glasses

U. Buchenau

*Forschungszentrum Jülich GmbH, Jülich Centre for Neutron Science
(JCNS-1) and Institute for Complex Systems (ICS-1), 52425 Jülich, Germany*

(Dated: October 20, 2020)

The strain field surrounding the center of low frequency vibrational modes in a glass is analyzed for numerically created binary glasses with a $1/r^{10}$ repulsive interatomic potential. Outside the unstable inner core of twenty to thirty atoms, one finds a mixture of a motion similar to the string motion in the core with the strain field of three oscillating elastic dipoles in the center. The additional outside string motion contributes more to the stabilization of the core than the strain field. The average creation energy of a soft mode in this binary glass is about 2.5 times the thermal energy at the freezing temperature. The elastic dipole field predicts a damping for the longitudinal sound waves at the boson peak in quantitative agreement with x-ray Brillouin data in a metallic glass.

PACS numbers:

Low frequency localized vibrations in glasses are traditionally thought to be intimately related to the tunneling states [1] and other low temperature glass anomalies like the plateau in the thermal conductivity and the boson peak [2–7]. At present, they are heavily studied numerically in binary glasses [8–16], the numerical counterpart of metallic glasses [17]. In these studies, the vibrational eigenmodes have a density increasing with the fourth power of their frequency and are localized to about twenty to hundred atoms, as long as their frequency is lower than the one of the lowest frequency sound wave fitting into the periodic boundary conditions of the simulation cell.

The core of the modes shows a string motion of the atoms with the largest amplitude [3] and is unstable [5, 7, 12]. Its saddle point configuration in energy is stabilized by positive restoring forces from the surroundings. The details of this stabilization are not yet well known. The present paper intends an analysis of this balance between inner and outer forces.

The analysis was done on twenty soft modes calculated by the Amsterdam group [8, 9, 11, 15] for a 50:50 binary mixture of atoms with the 3DIPL potential, a $1/r^{10}$ repulsive potential with an appropriate cutoff to avoid discontinuities in the derivatives. In terms of the potential energy E_0 , the modes were frozen in at a glass temperature T_g with $k_B T_g = 0.5 E_0$. In the freezing, the atomic volume V_a was held constant at $1.22 a_0^3$, where a_0 is the length unit (87 percent of the average nearest neighbor distance). The mass unit M is 1 for both kinds of atoms. The frozen glasses have a bulk modulus B of $56 E_0/a_0^3$ and a shear modulus G of $14 E_0/a_0^3$, leading to a transverse sound velocity of $4.12 E_0^{1/2} M^{-1/2}$, a longitudinal sound velocity of $9.52 E_0^{1/2} M^{-1/2}$, and a Debye frequency ω_D of $17.2 E_0^{1/2} M^{-1/2}/a_0$. Ten of the modes were normal modes in a cell of 16000 atoms, the other ten were quartic modes [9] in a cell of 128000 atoms.

To find the center of the mode, one first looks for atom 1 with the largest eigenvector amplitude \vec{e}_1 . One takes a sphere of radius $3.5 a_0$ (about three nearest neighbor distances) around this atom, containing a number N of

about hundred and forty atoms, and calculates a new center \vec{R}_0 with

$$\vec{R}_0 = \sum_{i=1}^N \vec{r}_i \vec{e}_i^2 / \sum_i \vec{e}_i^2, \quad (1)$$

where \vec{r}_i and \vec{e}_i are the position vectors and the eigenvector amplitudes of the inner core atoms, respectively.

Iterating this procedure around the new center three times, one finds a mode center which does not change any longer, and which is always closer than a_0 to the starting point. The core defined in this way contains about sixty percent of the normalized squared eigenvector for most modes.

For a given core radius r_c around this center, one can calculate the energy of the core atoms as a function of the mode coordinate by calculating their interaction energy with the other atoms in the core and with those atoms in the outer shell which are still within the interaction range (for the 3DIPL potential about $2a_0$).

Fig. 1 shows this energy dependence for the normal mode m3 with the core radius $1.9a_0$, containing 21 atoms. The instability of the core is clearly seen, as well as a pronounced linear potential term. The dependence is well fitted in terms of the soft potential function [2, 4], a

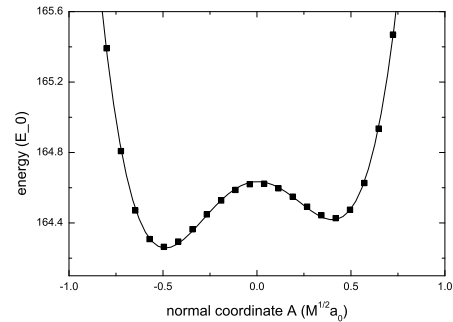


FIG. 1: Potential energy for the core of mode m3 with radius $r_c = 1.9a_0$. The line is a soft potential fit in terms of eq. (2).

polynomial up to fourth order in A

$$E(A) = E(0) + D_1A + D_2A^2 + D_3A^3 + D_4A^4, \quad (2)$$

where A is the normal coordinate, defined by the kinetic energy $E_{kin} = \dot{A}^2/2$ of the mode.

With increasing r_c , D_4 saturates to a constant value, for most of the modes below $r_c = 2.5a_0$, so this value can be taken as the beginning of the stabilizing outside, where the negative $D_2(r_c)$ begins to increase toward the small positive restoring force of the whole mode. This is shown in Fig. 2 for the same mode m3 as in Fig. 1. The arrow marks the boundary between inside and outside.

The simplest explanation for this decrease is an elastic distortion of the surrounding elastic medium [7] which is proportional to the normal coordinate A and which provides the positive restoring forces holding the unstable core on its saddle point in energy. It has recently been shown [18] that one can understand the surprisingly strong temperature dependence of the boson peak frequency in the glass phases of silica [19] and polycarbonate [20] in terms of this concept, postulating an unstable core also for the boson peak modes.

For the numerical modes, one can check whether this is indeed the correct explanation by fitting the mode displacements within an outer shell with shell radius r_s and the thickness d by an elastic dipole tensor proportional to A in the core center [21, 22]. Such an elastic dipole tensor gives rise to an atomic displacement decreasing with $1/r_s^2$, leading to a mean square shell displacement $\langle u^2 \rangle_{shell}$ decreasing proportional to $1/r_s^4$. The elastic displacement vector \vec{s} can be calculated from the elastic Greens function

$$G_{ij}(\vec{r}) = \frac{1}{8\pi G} \left(\frac{\delta_{ij}(1+f)}{r} + \frac{x_i x_j (1-f)}{r^3} \right) \quad (3)$$

where

$$f = \frac{3G}{3B+4G} = \frac{v_t^2}{v_l^2}. \quad (4)$$

δ_{ij} is the Kronecker symbol, x_i and x_j are cartesian components of the position vector \vec{r} . The displacement vector \vec{s} is given by

$$\vec{s}_i(\vec{r}) = - \sum_{j,k=1}^3 \frac{\partial G_{ij}}{\partial x_k} P_{jk}, \quad (5)$$

where the P_{jk} are the six components of the symmetric elastic dipole tensor in the center of the core.

But if one does these fits, one finds that the outside elastic response is only part of the explanation, the smaller part as far as the stabilization of the inner core on its saddle point in energy is concerned. The elastic dipole tensor displacements dominate at large distances from the core, but at smaller distances they are overshadowed by another more random kind of motion. This is demonstrated in Fig. 3, which shows the product $\langle u^2 \rangle_{shell} r_s^4$

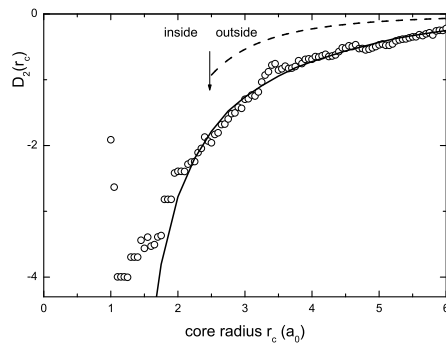


FIG. 2: Negative restoring force constant D_2 as a function of the core radius r_c for the same mode m3. Dashed line is $D_2(r_c)$ for only elastic outside restoring forces, continuous line elastic plus additional restoring forces from random modes outside the core (see text).

for consecutive shells of mode m3 with $d = 0.5$. The dashed line is the dipole tensor contribution. The elastic part of the positive restoring force contribution can be calculated with the elastic Greens function [21, 22]. For the simplest case of an expansion $\delta V/V$ of the core volume, one finds the outside energy $2GV(\delta V/V)^2/3$ of the shoving model [23], for a pure shear or a single dipole distortion of the core an energy which is a factor 1.22 larger for the same sum of squares of the P_{jk} (the factor 1.22 is calculated for the Poisson ratio 0.384 of the 3DIPL potential, close to the average Poisson ratio of 31 metallic glasses [17]). If this elastic force were the only positive restoring force from the outside (and if the frequency of the mode were exactly zero), $D_2(r_c)$ should follow the dashed line in Fig. 2.

The dipole tensor fit is reliable, because it yields the same six tensor elements within experimental error for different shell diameters r_s , if they are larger than $6a_0$ and still small compared to the distance of the dipole tensor in the neighboring periodic cell ($26.9 a_0$ for the cell with 16000 atoms). By a suitable rotation of the

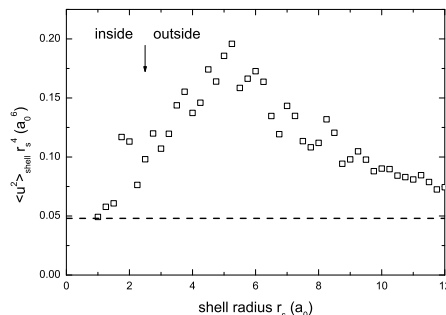


FIG. 3: Product of mean square displacement $\langle u^2 \rangle_{shell}$ with the fourth power of the shell radius r_s for consecutive shells of mode m3 with a shell thickness of $0.5 a_0$, showing the excess mean square displacement over the elastic one (the dashed line).

coordinate system, one can diagonalize the tensor and describe it by its three diagonal elements P_{11} , P_{22} and P_{33} . In the rotation, the new x -axis was chosen in the direction of largest expansion and the new y -axis along the direction of the strongest contraction. Looking at the tabulated values in Table I, one realizes that the elastic distortion component of the motion is essentially a shear, because the sum of the three diagonal elements is small for all investigated modes.

One can subtract the elastic dipole displacement to study the more random motion. After subtracting, one finds that the radial component of the outside mean square displacement still remains closer to 1/2 of the total than to the 1/3 of a completely random motion. Also, neighboring atoms still tend to move together, especially when they move along the line connecting them. Thus the more random component of the outside motion shows the string character first observed around the atom with the largest displacement in the inner core [3], suggesting that one has a similar kind of motion inside and outside, with the difference that the average restoring force is negative inside and positive outside.

To describe the measured $D_2(r_c)$ in Fig. 2, it is natural to assume that the energy of the more random component is not proportional to the derivative of the displacement (as in the elastic dipole component), but rather proportional to the mean square displacement $\langle u^2 \rangle_r$ of the more random component itself, with the (adaptable) proportionality factor f_r . Then its contribution to $D_2(r_c)$ is given by

$$D_{2r}(r_c) = -4\pi f_r \int_{r_c}^{\infty} \langle u^2 \rangle_r r_s^2 dr_s. \quad (6)$$

Adding this to the dashed line in Fig. 2 with $f_r = 1.3$, one gets the continuous line, which describes $D_2(r_c)$ very well, at least as long as one does not enter the inner core below $r_c \approx 2.5a_0$. One concludes that the larger part of the stabilizing outside restoring force is not due to the elastic distortion, but rather to the interaction with other string-like modes, proportional to their mean square displacement.

Naturally, one is dealing here with orthogonal modes which do not have a bilinear coupling between them. But this does not exclude bilinear interactions between different soft spots which then enter the eigenvector of the resulting orthogonal modes and show up in the present analysis.

f_r is an average restoring force of the more random modes surrounding the core, to be compared with the restoring force $\omega_D^2/2 = 147.9$ of the Debye frequency. Table I shows that it varies between 1.3 and 4.6 from mode to mode, showing that these modes come from a broad frequency band between one tenth and one fifth of the Debye frequency, in metallic glasses the frequency region from 2.5 to 5 meV at or slightly above the boson peak [24–26]. For the modes in Table I, they always supply at least two thirds of the stabilizing restoring forces.

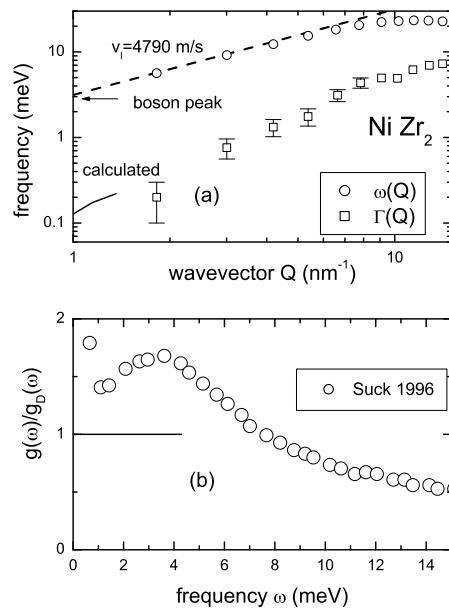


FIG. 4: (a) Frequency and damping of longitudinal sound waves measured by x-ray Brillouin scattering [28] in NiZr₂ compared to the calculation with the numerical coupling at the boson peak (b) Boson peak in NiZr₂ measured by inelastic neutron scattering [24] and normalized to the Debye density of states as described in the text.

On the other hand, the elastic distortion dominates at long distances, and so determines the bilinear coupling of the mode to an external strain

$$E_{bilinear} = P_{11}\epsilon_{11}A + P_{22}\epsilon_{22}A + P_{33}\epsilon_{33}A. \quad (7)$$

Of the five possible shears ϵ_t for a transverse sound wave, only two interact with the diagonal dipole tensor, namely the one with $\epsilon_{11} = -\epsilon_{22} = \epsilon_t/2$ and the other with $2\epsilon_{11} = 2\epsilon_{22} = -\epsilon_{33} = \epsilon_t/\sqrt{3}$. Averaging the squares, one finds an average bilinear transverse sound wave coupling $\lambda\epsilon_t A$ with

$$\lambda_t^2 = \frac{1}{15}(P_{11}^2 + P_{22}^2 + P_{33}^2 - P_{11}P_{22} - P_{22}P_{33} - P_{33}P_{11}). \quad (8)$$

The longitudinal strain ϵ_l is the combination of an expansion ϵ_l with the shear strain $4\epsilon_l/3$, so in the bilinear longitudinal sound wave coupling $\lambda_l\epsilon_l A$

$$\lambda_l^2 = (P_{11} + P_{22} + P_{33})^2 + \frac{16}{9}\lambda_t^2. \quad (9)$$

For the ten normal modes in Table I, one finds average values of $29.5 E_0/A$ for λ_l and $21 E_0/A$ for λ_t . The ratio λ_l/λ_t is 1.4, close to the value $4/3$ for a pure shear distortion and only slightly smaller than the ratio 1.6 found for tunneling states in a data collection [27].

To compare the numerical results to experimental data in metallic glasses, one can calculate the damping of the longitudinal sound waves at the boson peak from

$$\Gamma(\omega) = \frac{3\pi}{2} \frac{\lambda_l^2}{Mv_l^2} g_{exc}(\omega), \quad (10)$$

mode	f_r	P_{11}	P_{22}	P_{33}	E_s	ΔA	Ne	D_4
	E_0/A^2	E_0/A	E_0/A	E_0/A	E_0	A		E_0/A^4
m0	3.5	41	-55	7	1.7	1.0	17.6	9.3
m1	2.0	52	-49	2	0.5	0.9	65.8	4.0
m2	2.5	39	-54	9	0.9	1.0	16.6	20.5
m3	1.3	48	-53	19	0.9	1.0	35.1	7.3
m4	4.0	45	-46	11	0.7	0.9	12.5	16.5
m5	3.5	22	-51	17	1.8	1.2	34.3	7.9
m6	3.9	45	-36	-20	0.4	0.7	11.1	21.1
m7	4.6	61	-55	-20	0.6	1.0	13.0	10.1
m8	2.2	29	-34	13	1.7	1.3	77.3	2.9
m9	3.6	35	-55	21	3.1	1.4	37.8	6.2
q0	4.2	46	-23	-5	2.5	1.0	50.6	6.6
q1	2.6	31	-39	8	1.3	0.9	43.8	4.2
q2	1.8	34	-31	-19	0.7	1.4	8.1	19.4
q3	1.7	51	-32	-15	0.4	1.0	38.2	7.9
q4	1.5	50	-36	25	0.7	1.0	36.0	6.3
q5	6.3	45	-58	-3			99.5	2.6
q6	2.0	46	-66	13	0.8	1.2	30.4	10.9
q7	4.0	40	-33	-10	2.3	1.0	21.5	6.1
q8	3.8	40	-33	-10	1.6	1.2	28.2	10.3
q9		92	-12	30			21.4	575

TABLE I: Results of the unstable core analysis for ten normal modes (m) and ten quartic modes (q). Note that A , the normal coordinate unit, is $M^{1/2}a_0$, so f_r is a squared frequency.

where $g_{exc}(\omega)$ is the excess density of states over the Debye density of states $g_D(\omega)$ given by $3\omega^2/\omega_D^3$. $\Gamma(\omega)$ is the half width at half maximum of the Brillouin line. A nice feature of this equation is that is valid in both the soft potential model [2, 4] and Schirmachers fluctuating elasticity theory [6] (though in the fluctuating elasticity theory only approximate and with a prefactor proportional to the local elasticity fluctuations).

Fig. 4 (a) shows the comparison of measured x-ray Brillouin data [28] in the metallic glass NiZr₂ with this calculation. NiZr₂ has the longitudinal sound velocity 4790 m/s and the atomic volume 0.0188 nm³. Its transverse sound velocity has not been measured, but one finds the ratio $v_t^2/v_l^2 = 3/16$ of the 3DIPL potential in good approximation in Cu₅₀Zr₅₀Al₈ [29] and in Cu₄₆Zr₅₄ [17]. With this ratio, one calculates a Debye frequency of 22.5 meV for NiZr₂. The ratio λ_l^2/Mv_l^2 is a squared frequency and scales with the square of the Debye frequency.

The boson peak of NiZr₂ has been measured by inelastic neutron scattering [24] and is shown in Fig. 4 (b). For its normalization to the Debye density of states, its height of 1.65 $g_D(\omega)$ was taken over from low temperature heat capacity measurements [30] in Cu₅₀Zr₅₀Al₈.

With this normalization, the short line on the left of Fig. 4 (a) was calculated (one cannot go beyond 4.3 meV, because the Debye density of states is bound to fall below its zero frequency value at higher frequency). Within the error bars of the Brillouin x-ray measurement [28], the measured damping extrapolates to the calculated line, showing that the excess modes at the boson peak of this metallic glass have the same coupling to external strains as the numerical low frequency modes of the 3DIPL po-

tential.

The measurement of the boson peak in Fig. 4 (b) was done at two temperatures [24], at 296 K and 400 K. Unlike silica [19] and polycarbonate [20], NiZr₂ shows no visible temperature dependence of the boson peak. The shear modulus of a similar metallic glass, Vit4, diminishes [31] by 2.6 percent by heating from 296 K to 400 K, a change which in silica would shift the boson peak downward by seven percent. The measurement [24] in NiZr₂ excludes such a strong shift.

But the concept of a strong negative spring inside the core of the boson peak modes might still be correct. Compared to modes at the Debye frequency, they have a restoring force close to zero, suggesting the same compensation mechanism as in the numerical modes. The difference between silica and a metallic glass lies in the negative inner spring. In silica, it is a rotation of coupled SiO₄ tetrahedra [19], and its temperature dependence need not be the same as the one of the elastic constants, while the string motion resembles the one of a transverse zone boundary mode, with a Grüneisen parameter close to the one of the transverse sound waves. If both the negative spring inside and the positive spring outside have the same temperature dependence, the resulting boson peak frequency shift will not be anomalous.

A comparison of the numerical results to the tunneling plateau of another metallic glass at low temperatures will be done in a future publication [32].

The last step is to estimate the creation energy of the soft modes, allowing the core atoms to find their energy minimum for a given mode displacement of the outer atoms, by an appropriate variation of the core atom positions and an adaptation of the mode displacement of the outer atoms. In this way, one can find the minimum packing energy of the core atoms for the given density. The difference between this minimum packing energy and the energy at displacement zero provides the frozen saddle point energy E_s , the creation energy of the soft mode. The calculations were done for the core radius $r_c = 2.6a_0$. The analysis was not done for mode q5, where D_4 saturates very late, at 4.4 a_0 , and also not for mode q9, which had no unstable core and a very large D_4 .

It turns out that this minimum of the packing energy occurs for a relatively large displacement of the outer atoms along the mode coordinate, about 1.5 times larger than the displacement for the minima in Fig. 1. About eighty percent of the atomic motion inside is a backward motion along the mode coordinate, bringing the inside mode displacement down to the ΔA in Table I, about two thirds of the outside value. The accurate determination of the two minimal energies in both directions requires the subtraction of the linear potential term. The average creation energy is 1.25 E_0 (2.5 $k_B T_g$) for both the normal modes and the quartic modes, in reasonable agreement with the recent theoretical estimate 3.22 $k_B T_g$ on the basis of an atomic model of the motion [33]. It explains the strong reduction in the number of soft modes in glasses [14] cooled to low glass temperatures with the

swap mechanism [34].

In this context, it should be mentioned that the string motion was not only found in the soft modes and low temperature relaxations [3], but also in the relaxational motion at the glass transition [35] (without mentioning the earlier glass work). The finding supports the recent explanation of the highly viscous flow [33] in terms of the creation and annihilation of soft modes.

Finally, Table I lists the two parameters usually characterizing the soft modes in the numerical world, the number N_e of atoms in the mode, calculated from the participation ratio e (the inverse of the sum over the square of the squared eigenvector for all N atoms in the simulation

cell) and the fourth order term D_4 .

To summarize, the analysis of the positive restoring forces outside the inner unstable core of soft vibrational modes in numerically cooled binary glasses allows to separate a smaller part due to the elastic distortion and a larger part due to the interaction with other soft spots outside the core. The smaller elastic part enables a soft potential prediction for the absorption of longitudinal sound waves at the boson peak in quantitative agreement with x-ray Brillouin data in a metallic glass.

Thanks are due to Edan Lerner for supplying the twenty soft modes and helpful suggestions.

-
- [1] W. A. Phillips, Rep. Prog. Phys. **50**, 1657 (1987)
- [2] U. Buchenau, Yu. M. Galperin, V. L. Gurevich, D. A. Parshin, M. A. Ramos and H. R. Schober, Phys. Rev. B **46**, 2798 (1992)
- [3] H. R. Schober, C. Oligschleger, and B. B. Laird, J. Non-Cryst. Solids **156-158**, 965 (1993)
- [4] M. A. Ramos and U. Buchenau, Phys. Rev. B **55**, 5749 (1997)
- [5] V. A. Luchnikov, N. N. Medvedev, Yu. J. Naberukhin, and H. R. Schober, Phys. Rev. B **62**, 3181 (2000)
- [6] W. Schirmacher, G. Ruocco, and T. Scopigno, Phys. Rev. Lett. **98**, 025501 (2007)
- [7] U. Buchenau and H. R. Schober, Phil. Mag. **88**, 3885 (2008)
- [8] E. Lerner, G. Düring, and E. Bouchbinder, Phys. Rev. Lett. **117**, 035501 (2016)
- [9] L. Gartner and E. Lerner, SciPost **1**, 016 (2016)
- [10] S. Wijtmans and M. L. Manning, Soft Matter **13**, 5649 (2017)
- [11] G. Kapteijns, E. Bouchbinder, and E. Lerner, Phys. Rev. Lett. **121**, 055501 (2018)
- [12] M. Shimada, H. Mizuno, M. Wyart, and A. Ikeda, Phys. Rev. E **98**, 060901 (2018)
- [13] H. Mizuno and A. Ikeda, Phys. Rev. E **98**, 062612 (2018)
- [14] L. Wang, A. Ninarello, P. Guan, L. Berthier, G. Szamel, and E. Flenner, Nat. Commun. **10**, 26 (2019)
- [15] G. Kapteijns, D. Richard, and E. Lerner, arXiv:1912.10930
- [16] D. Coslovich, A. Ninarello, and L. Berthier, SciPost Phys. **7**, 077 (2019)
- [17] W.L. Johnson and K. Samwer, Phys. Rev. Lett. **95**, 195501 (2005)
- [18] U. Buchenau, arXiv:1907.04848
- [19] A. Wischnewski, U. Buchenau, A. J. Dianoux, W. A. Kamitakahara, and J. L. Zarestky, Phys. Rev. B **57**, 2663 (1998)
- [20] U. Buchenau, C. Schönfeld, D. Richter, T. Kanaya, K. Kaji, and R. Wehrmann, Phys. Rev. Lett. **73**, 2344 (1994)
- [21] G. Leibfried and N. Breuer, *Point Defects in Metals I*, Vol. 81 of Springer Tracts in Modern Physics (Springer, Berlin 1981)
- [22] E. Clouet, C. Varvenne, and Th. Jourdan, Comp. Mat. Sci. **147**, 49 (2018)
- [23] J. C. Dyre, N. B. Olsen, and T. Christensen, Phys. Rev. B **53**, 2171 (1996)
- [24] J.-B. Suck, J. Non-Cryst. Solids **205-207**, 592 (1996)
- [25] A. Meyer, J. Wuttke, W. Petry, A. Peker, R. Bormann, G. Coddens, L. Kranich, O. G. Randl, and H. Schober, Phys. Rev. B **53**, 12107 (1996)
- [26] A. Meyer, J. Wuttke, W. Petry, O. G. Randl, and H. Schober, Phys. Rev. Lett. **80**, 4454 (1998)
- [27] J. F. Berret and M. Meissner, Z. Phys. B - Condensed Matter **70**, 65 (1988)
- [28] T. Scopigno, J.-B. Suck, R. Angelini, F. Albergamo, and G. Ruocco, Phys. Rev. Lett. **96**, 135501 (2006)
- [29] Y. Li, P. Yu, and H. Y. Bai, Appl. Phys. Lett. **86**, 231909 (2009)
- [30] Y. Tian, Zh. Q. Li, E. Y. Jiang, Solid State Commun. **149**, 1527 (2009)
- [31] M. L. Lind, G. Duan, and W. L. Johnson, Phys. Rev. Lett. **97**, 015501 (2006)
- [32] U. Buchenau, G. D'Angelo, G. Carini, X. Liu and M. A. Ramos (unpublished).
- [33] U. Buchenau, arXiv:2003.07246
- [34] A. Ninarello, L. Berthier, and D. Coslovich, Phys. Rev. X **7**, 021039 (2017)
- [35] C. Donati, J. F. Douglas, W. Kob, S. J. Plimpton, P. H. Poole, and S. C. Glotzer, Phys. Rev. Lett. **80**, 2338 (1998)